JOURNAL OF THERMOPHYSICS AND HEAT TRANSFER
Vol. 6, No. 3, July–Sept. 1992

Thermal Radiation Effects on a Shocked Particle-Laden Gas

J. L. Haferman,* R. G. Schmitt,* T. F. Smith,† and P. B. Butler‡
University of Iowa, Iowa City, Iowa 52242

A mathematical model is presented that describes the particle-gas interactions that occur when a shock wave propagates through a particle-laden gas. In most of the previous work in this field, thermal radiation was neglected when solving the energy conservation equation throughout the shock relaxation zone. The present study represents an extension of the previous analyses to include thermal radiation in the governing conservation equations. The present analysis focuses on the dynamic and thermodynamic events taking place within the domain of the relaxation zone, as well as the coupling of the relaxation zone and the preheat zone. Viewed in a shock-fixed coordinate system, the preheating and relaxation zones each have a constant length (steady-state assumption) for specified conditions and, for convenience, all properties within each zone can be referenced to the distance from the shock front. The results presented show the influence of thermal radiation on shock wave structure, and predict the distance ahead of the shock front that thermal radiation penetrates the particle-laden gas, thereby providing preshock heating to both the particles and the gas.

Nomenclature

a_n = nth coefficient of specific heat polynomial function, K^{-n}
C_D = drag-force coefficient
C_{Pg} = gas-component specific heat at constant pressure, J/kg-K
C_{Pp} = particle specific heat, J/kg-K
C_{vg} = gas-component specific heat at constant volume, J/kg-K
d = particle diameter, m
E = specific total energy, J/kg
F = intercomponent drag force per particle, N
h = convective heat transfer coefficient, W/m²-K
I = radiant intensity, W/m²-sr
k = thermal conductivity, W/m-K
L_{sh} = preshock heating zone length, m
L_{Te} = temperature relaxation zone length, m
M = Mach number, $V_0(\gamma RT_0)^{1/2}$
M_w = molecular weight, kg/kmole
m = mass, kg
Nu = Nusselt number, hd/k
P = gas pressure, N/m²
Pr = Prandtl number, $C_{Pg}\mu/k$
Q = intercomponent convective heat transfer per particle, W
Q_a = absorption efficiency factor
Q_s = scattering efficiency factor
q_r = radiative heat flux, W/m²
R = gas constant, J/kg-K
$\bar{R}$ = universal gas constant, 8314.3 J/kmol-K
Re = Reynolds number, $\rho ud/\mu$
T = temperature, K
V = velocity relative to shock from, m/s
V_0 = shock velocity, m/s
X = shock-fixed coordinate, m
γ = specific heat ratio, C_{Pg}/C_{vg}
δ = increment of shock location, m
ε_e = temperature error at equilibrium state
ε_o = particle temperature gradient at initial state, K/m
η = mass-flow ratio
θ_g, θ_p = dimensionless gas and particle temperature, T/T_0
κ = absorption coefficient, m^{-1}
μ = viscosity, kg/m-s
ρ = density, kg/m³
σ = Stefan-Boltzmann constant, 5.669×10^{-8} W/m²-K⁴
σ_p = particle concentration, kg/m³
σ_s = scattering coefficient, m^{-1}
ϕ_g = gas volume-fraction, $1 - \phi_p$
ϕ_p = particle volume-fraction
Ω = relaxation factor
ω = single scattering albedo

Subscripts

a = absence of radiation
b = blackbody
e = equilibrium condition
f = frozen condition
g = gas
m, n = iteration counters
o = initial condition
p = particle
$+$ = high pressure side of shock front
$-$ = low pressure side of shock front

Superscripts

$-$ = intensity directed in negative x direction
$+$ = intensity directed in positive x direction

Introduction

OVER the years, several different approaches have been taken to develop a mathematical model that describes the particle-gas interactions that occur when a shock wave propagates through a particle-laden gas. These included studies on both nonreactive and reactive mixtures. The early work of Carrier[1] represents the first attempt at presenting a simplified form of the governing conservation equations for a particle-laden gas following a normal shock wave. Others contributing to the continuing development and analysis over the years include: Zink,[2] Campbell and Pitcher,[3] Morgenthaler,[4] Kriebel,[5] Rudinger,[6–9] Varma and Chopra,[10] Krier and Mozaffarian,[11] Elperin et al.,[12] Ben-Dor and Igra,[13] Igra and Ben-Dor,[14] Rakib et al.,[15] Yao,[16] Butler and Schmitt,[17] and Baek and Seung.[18,19] In most of the previous work in this field,

Received Jan. 28, 1991; revision received May 17, 1991; accepted for publication May 30, 1991.

*Graduate Student, Department of Mechanical Engineering.
†Professor, Department of Mechanical Engineering. Member AIAA.
‡Associate Professor, Department of Mechanical Engineering. Member AIAA.

thermal radiation was neglected when solving the energy conservation equation throughout the shock relaxation zone. The present study represents an extension of the prior analyses to include thermal radiation in the governing conservation equations.

In summary, the primary objective of this study is to examine the relaxation zone structure of a nonreactive, particle-laden gas that is thermally radiative. Specifically, the analysis predicts the temperature, velocity, pressure, and particle concentration distributions for the gas and particle components. Other important parameters resulting from the analysis are the distances relative to the shock front at which particles come into temperature and velocity equilibrium with the gas-component. The results presented here also show the influence of thermal radiation on shock wave structure and predict the distance ahead of the shock front that thermal radiation penetrates the particle-laden gas, thereby providing preshock heating to both the particles and gas.

Analysis

System Description

A schematic diagram of a duct with a normal shock wave is illustrated in Fig. 1, where X is a shock-fixed coordinate. In this figure, monodispersed, micron-sized particles are suspended in the gas. It is generally assumed that when a normal shock wave propagates through a particle-laden gas, the particles pass through the shock front momentarily unaffected. This is a reasonable assumption when considering the particle-component momentum and energy balances across the thickness of the gas-component shock wave. That is, the time- (or length-) scale of the shock front is much too short to produce any significant changes in the thermodynamic state of the particles. Although the particles are not immediately influenced by the shock wave, the gas-component (viewed in a shock-fixed coordinate system) is always shocked to a higher temperature and pressure and lower velocity. This creates velocity and temperature differences between the two components and, consequently, initiates intercomponent momentum and energy transfer to re-equilibrate the gas/particle mixture. The region between the shock front and the location where the mixture returns to complete thermal and mechanical equilibrium is termed the "relaxation zone." Likewise, the region that is in front of the shock wave is influenced thermally by events occurring within the relaxation zone and is appropriately referred to as the "preheat zone." The present analysis focuses on the dynamic and thermodynamic events taking place within the domain of the relaxation zone, as well as the coupling of the relaxation zone and the preheat zone. Viewed in a shock-fixed coordinate system X, the preheating and relaxation zones each have a constant length (steady-state assumption) for specified conditions and, for convenience, all properties within each zone can be referenced to the distance from the shock front. In Fig. 1, the preheat zone extends from $X = 0$ to $X = X_f$, and the relaxation zone extends from X_f to X_e. Radiant intensities of I^+ and I^- are sketched in Fig. 1 to illustrate propagation of radiant energy. Further discussion of this is given later.

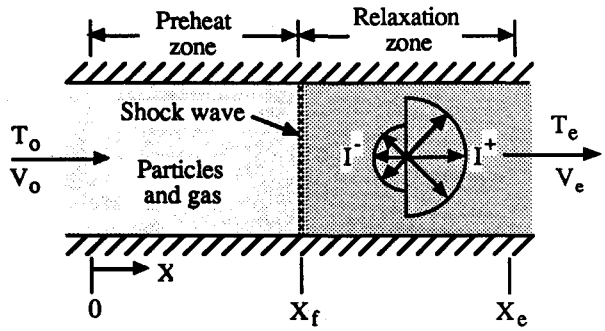

Fig. 1 Shock wave system.

Locations $X = 0$ and $X = X_e$ are sufficiently removed from the shock wave so that the gas and particles are in thermal and mechanical equilibrium at these locations. The flow is steady, one-dimensional, enters at the left at temperature T_0 and velocity V_0, and exits at the right at temperature T_e and velocity V_e, where the velocities are relative to the shock-wave velocity. The temperature distribution within the particles is uniform, and chemical reaction effects are neglected. The volume occupied by the particle-component is negligible (low particle loading). In addition, the particles are assumed to be incompressible spheres, to absorb, emit, and scatter radiant energy, and to be radiatively gray.

The gas-component is assumed to follow the ideal-gas equation of state, to be a one-dimensional, continuum flow, and to be radiatively transparent. The gas is further assumed to be inviscid except for the drag force exerted on the particles, and it is assumed that there is no heat transfer within the gas. The gas-component jump conditions across the shock front are calculated using the Rankine-Hugoniot relations with temperature-dependent specific heats. The jump conditions across the shock front are assumed to be unaffected by the presence of particles. This assumption is reasonable given the extremely low volume-fraction of particles common to mixtures of interest in this study.

Governing Equations

Following the earlier work of Krier and Mozaffarian,[11] Yao,[16] and Butler and Schmitt,[17] the governing equations for the gas/particle mixture are derived using a separated, two-component flow analysis. In deriving the equations, the particle volume-fraction is assumed small enough that the particles do not interfere with one another. For a control volume element, conservation conditions can be expressed for the mass, momentum, and energy of both the gas and particle components. The resulting conservation equations form a system of partial differential equations with space and time as the independent variables. The total number of equations is six because there are continuity, momentum, and energy equations for the gas-component and the particle-component.

In this study, the preheat and shock relaxation zones are viewed as a steady-state system moving with the shock front at velocity V_0 (see Fig. 1). Thus, a coordinate system that is fixed to the shock front can be defined. The steady-state forms of the governing equations in transformed shock coordinates are

Gas Continuity

$$\frac{d}{dX}[\phi_g \rho_g V_g] = 0 \tag{1}$$

Particle Continuity

$$\frac{d}{dX}[\phi_g \rho_g V_p] = 0 \tag{2}$$

Gas Momentum

$$\frac{d}{dX}[\phi_p \rho_p V_g^2] + \phi_g \frac{dP}{dX} = \frac{\phi_p \rho_p F}{m_p} \tag{3}$$

Particle Momentum

$$\frac{d}{dX}[\phi_p \rho_p V_p^2] + \phi_p \frac{dP}{dX} = -\frac{\phi_p \rho_p F}{m_p} \tag{4}$$

Gas Energy

$$\frac{d}{dX}[\phi_g \rho_g E_g V_g] + \frac{d}{dX}[\phi_g P V_g] = \frac{\phi_p \rho_p}{m_p}[F V_p - Q] \tag{5}$$

Particle Energy

$$\frac{\mathrm{d}}{\mathrm{d}X}[\phi_p\rho_p E_p V_p] + \frac{\mathrm{d}}{\mathrm{d}X}[\phi_p P V_p] = \frac{\phi_p\rho_p}{m_p}[Q - FV_p] - \frac{\mathrm{d}q_r}{\mathrm{d}X} \tag{6}$$

where V_g and V_p are the component velocities relative to the shock front, respectively. In Eqs. (1–6), ϕ_p is the particle volume-fraction, ϕ_g is the gas volume-fraction, P is the pressure, ρ_g is the gas density, ρ_p is the particle density, m_p is the particle mass, F is the intercomponent drag force, Q is the intercomponent convective heat transfer, and E represents the specific total (kinetic and internal) energy. The last term appearing in Eq. (6) $\mathrm{d}q_r/\mathrm{d}X$ is a volumetric radiative heat flux commonly called the divergence of the radiative heat flux. The specific total energy of the particle-component is represented by

$$E_{px} = \int_0^{T_x} C_{P_p}(T)\,\mathrm{d}T + \frac{1}{2}V_{px}^2 \tag{7}$$

where subscript x refers to the state at which the energy is desired and C_{P_p} is the specific heat of the particle-component. Similarly, the specific total energy of the gas-component is

$$E_{gx} = \int_0^{T_x} C_{vg}(T)\,\mathrm{d}T + \frac{1}{2}V_{gx}^2 \tag{8}$$

where C_{vg} is the constant-volume specific heat of the gas-component.

In order to solve numerically Eqs. (1–6), a differential operator form of the equations is derived using the conservation equations for the shock coordinate system in addition to the ideal-gas equation of state. For this study, the particle volume-fraction is assumed to be negligible (i.e., $\phi_p \approx 0$). However, the particle concentration ($\sigma_p = \phi_p\rho_p$) is retained in the final form of the equations to account for the influence of the particle-component on the flow conditions. The differential operator forms of the equations are

Particle Velocity

$$\frac{\mathrm{d}V_p}{\mathrm{d}X} = -\frac{F}{V_p m_p} \tag{9}$$

Particle Temperature

$$\frac{\mathrm{d}T_p}{\mathrm{d}X} = \frac{\dfrac{Q}{m_p} - \dfrac{1}{\sigma_p}\dfrac{\mathrm{d}q_r}{\mathrm{d}X}}{V_p C_{P_p}} \tag{10}$$

Gas Velocity

$$\frac{\mathrm{d}V_g}{\mathrm{d}X} = \frac{\dfrac{\sigma_p F}{\rho_g m_p} - R\dfrac{\mathrm{d}T_g}{\mathrm{d}X}}{\dfrac{V_g^2 - RT_g}{V_g}} \tag{11}$$

Gas Temperature

$$\frac{\mathrm{d}T_g}{\mathrm{d}X} = \frac{1}{\rho_g V_g}\left\{\frac{\dfrac{\sigma_p}{m_p}[FV_p - Q] - \dfrac{V_g^3}{V_g^2 - RT_g}\dfrac{\sigma_p F}{m_p}}{C_{Pg} - \dfrac{V_g^2 R}{V_g^2 - RT_g}}\right\} \tag{12}$$

Gas Density

$$\frac{\mathrm{d}\rho_g}{\mathrm{d}X} = -\frac{\rho_g}{V_g}\frac{\mathrm{d}V_g}{\mathrm{d}X} \tag{13}$$

Gas Pressure

$$\frac{\mathrm{d}P}{\mathrm{d}X} = R\left[\rho_g\frac{\mathrm{d}T_g}{\mathrm{d}X} + T_g\frac{\mathrm{d}\rho_g}{\mathrm{d}X}\right] \tag{14}$$

Particle Concentration

$$\frac{\mathrm{d}\sigma_p}{\mathrm{d}X} = -\frac{\sigma_p}{V_p}\frac{\mathrm{d}V_p}{\mathrm{d}X} \tag{15}$$

where R represents the gas constant. Intercomponent momentum and energy transfer is accounted for by the correlations[17]

Particle Drag

$$F = \frac{C_D}{2}\rho_g\left(\frac{\pi\,\mathrm{d}^2}{4}\right)|V_p - V_g|(V_p - V_g) \tag{16}$$

$$Re = \rho_g|V_g - V_p|\,\mathrm{d}/\mu \tag{17}$$

$$C_D = 0.48 + 28/Re^{0.85} \tag{18}$$

Exchange of Energy

$$Q = h(T_g - T_p)\pi\,\mathrm{d}^2 \tag{19}$$

$$h = k_g Nu/\mathrm{d} \tag{20}$$

$$Nu = 2 + 0.6\,Pr^{1/3}Re^{1/2} \tag{21}$$

Because of the range in temperatures experienced during the shock and re-equilibration processes, the specific heat at constant pressure of the gas-component and particle-component can be expressed as temperature-dependent polynomial functions of the form

$$C_P = \frac{\bar{R}}{M_w}\sum_{n=0}^{N} a_n T^n \tag{22}$$

where $\bar{R}$ is the universal gas constant, M_w is the molecular weight of the component, and the temperature coefficients a_n come from the standard JANAF thermochemical data base.[20] The temperature variation of the viscosity is taken from a power law curve fit to viscosity data.[21] A polynomial curve fit for air thermal conductivity data[21] is used for the temperature dependency of the gas thermal conductivity.

Equations (9–15) form a system of seven ordinary differential equations for the seven dependent variables (V_p, T_p, T_g, V_g, ρ_g, P, σ_p). In this formulation, the independent variable is the shock-fixed coordinate X. The governing equations are continuous over the preshock, preheat zone $0 < X < X_{f-}$ and over the postshock, re-equilibration zone $X_{f+} < X < X_e$. However, V_g, T_g, ρ_g, and P are discontinuous across the shock front $X_{f-} < X < X_{f+}$. Subscripts $-$ and $+$ refer to locations immediately before and after the shock front, respectively. Initial conditions for all the dependent variables are required at $X = 0$, and, because of the shock discontinuity at $X = X_f$, expressions for the "jump" conditions across the shock front are also necessary.

Rankine-Hugoniot Jump Conditions

In formulating the governing equations, a control volume analysis was applied to the two-component mixture. The resulting governing equations describe both the preshock zone and the relaxation zone directly behind the shock front. The relaxation zone extends from what is referred to as the "frozen" state X_{f+} to the equilibrium state X_e (Fig. 1). The frozen state is the condition immediately behind the shock front, after the gas is shocked to a higher temperature, pressure, and lower velocity (in shock coordinates). The frozen state

can be calculated using the Rankine-Hugoniot shock relations[9,11,17] for the gas-component alone. The "frozen" jump conditions are

Continuity

$$\rho_{g-} V_{g-} = \rho_{g+} V_{g+} \tag{23}$$

Momentum

$$\rho_{g-} V_{g-}^2 + P_- = \rho_{g+} V_{g+}^2 + P_+ \tag{24}$$

Energy

$$E_{pg-} = E_{pg+} \tag{25}$$

These equations do not represent a closed form solution to the variables at the + state and must be solved simultaneously. In addition, the frozen state jump conditions given by Eqs. (23–25) are coupled to the solution obtained at X_{f-} from evaluating the differential equations over the domain $0 < X < X_{f-}$.

Equilibrium State

As a means to verify the solution of the system of ordinary differential equations, the Rankine-Hugoniot shock relations are applied to the mixture of gas and particles to solve for the equilibrium state at $X = X_e$. The equilibrium Hugoniot solution is derived in a similar fashion as the frozen-state Hugoniot. Note that the specific heat is again modeled as a function of temperature. Integrating the governing equations between the initial and equilibrium states yields

Mixture Continuity

$$(\phi_{go}\rho_{go} + \phi_{po}\rho_p)V_0 = (\phi_{ge}\rho_{ge} + \phi_{pe}\rho_p)V_e \tag{26}$$

Mixture Momentum

$$(\phi_{go}\rho_{go} + \phi_{po}\rho_p)V_0^2 + P_0 = (\phi_{ge}\rho_{ge} + \phi_{ge}\rho_{pe}\rho_p)V_e^2 + P_e \tag{27}$$

Mixture Energy

$$E_{go} + \eta E_{po} + \eta \frac{P_0}{\rho_p} = E_{ge} + \eta E_{pe} + \eta \frac{P_e}{\rho_p} \tag{28}$$

In Eq. (28), η represents the ratio of mass flow of particles to mass flow of gas at the initial state

$$\eta = \sigma_p/\phi_{go}\rho_{go} \tag{29}$$

where $\phi_{go} \approx 1$ because $\phi_p \approx 0$. Similar to the frozen-state jump conditions, Eqs. (26–28) do not represent a closed form solution and must be solved simultaneously.

Radiation Model

For the one-dimensional system depicted in Fig. 1, the two-flux radiation model[22–24] is applicable. For this model, the intensity is considered to have a forward direct component I^+ in the positive X direction and a backward directed component I^- in the negative X direction, both of which are independent of direction as illustrated in Fig. 1. In view of the particle diameters and the temperature levels reported here, the radiant energy is mainly found at wavelengths shorter than 10 μm. Hence, the particle size parameter defined as the circumference of the particle divided by the wavelength is greater than five, which is near the lower end of the range for geometrical optics.[25] The particle scattering phase function is, therefore, highly peaked in the forward direction due to diffraction. To account for this peak, the scattering phase function is modeled as the sum of a Dirac-delta function for the forward direction and a scattered term that is assumed to be isotropic. The diffraction-subtraction method of Kamiuto[26] is used to account for this scattering phase function in the radiative transport equation.

Based on these statements, the forward and backward intensities are evaluated from the following two ordinary diffrential equations:

$$\frac{dI^+}{dX} = -(2\kappa + \sigma_s)I^+ + \sigma_s I^- + 2\kappa I_b \tag{30}$$

$$-\frac{dI^-}{dX} = -(2\kappa + \sigma_s)I^- + \sigma_s I^+ + 2\kappa I_b \tag{31}$$

where κ is the absorption coefficient and σ_s is the scattering coefficient for scattering that excludes the forward direction. Physically, the terms, in the order shown on the right side of Eqs. (30) and (31), could be interpreted as the absorbed and outward scattered radiant energy, the inward scattered radiant energy, and the radiant energy emitted in the considered direction. The boundary conditions for I^+ and I^- are given downstream and upstream of the shock wave. To state the boundary conditions, porous, black plugs are assumed to be positioned at $X = 0$ and X_e with respective temperatures of T_0 and T_e. The gas and particles flow unimpeded through the plugs. Thus

$$\text{at } X = 0, \quad I^+(0) = I_{b0} = \sigma T_0^4/\pi \tag{32}$$

and

$$\text{at } X = X_e, \quad I^-(X_e) = I_{be} = \sigma T_e^4/\pi \tag{33}$$

where σ denotes the Stefan-Boltzmann constant. The divergence of the radiative flux is defined as the difference between the emitted radiant energy and absorbed irradiation and is evaluated from

$$\frac{dq_r}{dX} = 4\kappa\sigma T_p^4 - 2\pi\kappa(I^+ + I^-) \tag{34}$$

Statements in Eqs. (30–34) provide a closure to obtain the solution to the governing equations, Eqs. (9–15).

The particles are spherical, monodisperse, and have wavelength- and temperature-independent properties. Under these conditions, the absorption and scattering coefficients are expressed by, respectively

$$\kappa = 1.5\, Q_a \phi_p/\mathrm{d} \tag{35}$$

$$\sigma_s = 1.5\, Q_s \phi_p/\mathrm{d} \tag{36}$$

where Q_a and Q_s are the absorption and scattering efficiency factors.[25] For the geometrical range, the absorption and scattering (excluding the diffraction peak) coefficients sum to unity. Thus, the radiative properties are expressed in terms of one parameter, taken here as the single scattering albedo ω. In terms of the scattering albedo, the scattering and absorption coefficients are given, respectively, by $Q_s = \omega$ and $Q_a = 1 - \omega$.

Numerical Procedure

The governing differential equations stated by Eqs. (9–15), Eqs. (30) and (31), and Eq. (34) are integrated numerically forward in the shock-fixed coordinate using LSODE,[27] an initial value solution scheme. Without radiation, the governing equations reduce to an initial value problem starting at the shock front. With radiation, a two-point boundary value problem is stated, due to the radiant intensity boundary conditions of Eqs. (32) and (33). To find the radiative flux, the intensity expressions given by Eqs. (30) and (31) with corresponding boundary conditions of Eqs. (32) and (33) must

be solved. However, the boundary condition for the backward intensity I^- is prescribed at the equilibrium plane $X = X_e$. Therefore, the initial value of $I^-(0)$ must be found in order for LSODE to solve the equations.

The solution for $I^-(0)$ is found by making use of the knowledge that the particles are in thermal equilibrium in the region far ahead of the shock front, that is

$$\left.\frac{dT_p}{dX}\right|_0 < \varepsilon_o \tag{37}$$

where the temperature gradient ε_o at $X = 0$ is typically assigned a value of 10^{-5} K/m. Setting Eq. (12) equal to ε_o at $X = 0$, inserting Eq. (32), and solving for $I^-(0)$ yield

$$I^-(0) = [\varepsilon_o \phi_p \rho_p V_p C_{P_p} + 2\kappa\sigma T_0^4]/2\pi\kappa \tag{38}$$

The boundary value problem has been transformed into an initial value problem that requires the location of the shock front to be specified.

With an initial guess for the location of the shock X_f, the governing equations can be solved from the initial state at $X = 0$ to the preshock state at X_{f-}, and from the post shock at X_{f+} to the equilibrium state at $X = X_e$. The discontinuity at X_f is evaluated using the Rankine-Hugoniot shock jump equations, Eqs. (23–25). Equilibrium is determined when the temperatures of the particle- and gas-components are nearly equal as stated by

$$(T_g - T_p)/T_g < \varepsilon_e \tag{39}$$

where $\varepsilon_e = 10^{-3}$.

Once the equilibrium state is determined, $I^-(X_e)$ can be compared with the boundary condition of Eq. (33). If the comparison fails, the assumed value for the location of the shock must be adjusted and the integration process repeated. The iteration procedure is repeated until the boundary condition is satisfied.

The procedure for determining appropriate values of X_f involves two steps. The first step is to find a value of $I^-(0)$ such that the integration does not exceed certain limits. The second step iterates on the value of X_f until convergence is obtained.

For the first step, an initial value of the shock front position, called $X_{f,o}$, is assumed. $I^-(0)$ is then calculated from Eq. (38), and the governing equations are integrated. If, in the integration process, $I^-(X) > I_{\max}$, where $I_{\max}$ is an upper limit for the intensity (typically about 10^6 W/m^2 – sr), the assumed value of X_f is too large. Here, the half-interval method is used to obtain a new estimate for the shock position by

$$X_{f,m+1} = X_{f,m}/2 \tag{40}$$

where subscript m refers to the iteration count for the first step. If instead $I^-(X) < I_{\min}$ (typically about -10^5 W/m^2 – sr), then the assumed value of X_f is too small and a new value for X_f is computed using

$$X_{f,m+1} = X_{f,m} + \Delta X \tag{41}$$

where $\Delta X = 1.0$ m. This procedure is repeated until $I_{\min} < I^-(X) < I_{\max}$ at which point the boundary condition on $I^-(X_e)$ can be checked, and the second step is initiated.

For the second step, the estimate for X_f is adjusted by employing the secant method.[28] At $X = X_e$, an intensity error ΔI^- between the boundary condition of Eq. (33) and the intensity furnished by the integration routine $I^-(X_e)$ is computed as

$$\Delta I_n^- = I_{be} - I^-(X_e) \tag{42}$$

where n is the iteration count for the second step. For the first evaluation, $n = 1$. The intensity error is viewed as a function of X_f; the purpose of the solution scheme is to minimize this error.

With ΔI_0^- computed, a second value of the shock location is computed using $X_{f,2} = X_{f,1}(1 + \delta)$, where $\delta = 0.005$, and ΔI_2^- is computed. With the second iteration completed, an updated estimate for the shock location for the next iteration is evaluated from

$$X_{f,n+1} = X_{f,n} - \Omega \frac{\Delta I_n^-(X_{f,n} - X_{f,n-1})}{\Delta I_n^- - \Delta I_{n-1}^-} \tag{43}$$

which is used when $n > 1$. The relaxation factor Ω is between 0 and 1 and is used to reduce the effects of nonlinearities so that solutions to highly nonlinear problems can be obtained. If any iteration produces a value of $I^-(X_e)$ that is less than $I_{\min}$ or greater than $I_{\max}$, the search method of Eqs. (40) and (41) is re-employed to reduce further the interval in which X_f is located.

The rate of convergence of this solution method is highly dependent on the selection of the radiation parameters, shock location, and relaxation factor. A converged solution is typically obtained within a dozen or so iterations. Some representative values of Ω and $X_{f,0}$ are given in Table 1, with the numerical results produced by the iteration scheme. This table is furnished as an aid to the reader for obtaining other solutions. The reader should be aware that judicious adjustment of $X_{f,0}$ and Ω may be necessary to obtain solutions when the radiation terms are present.

Once X_f is found, the depth that radiation penetrates into the preshock heating zone is determined. The preheating zone length L_{sh} is defined as the distance from the shock front to the point ahead of the shock where the temperature gradient of the particle-component is equal to 10^{-3} K/m. This distance is independent of the value chosen for ε_o when ε_o is less than 10^{-4} K/m.

Results

As mentioned previously, the primary objective of this study is to examine the preheat and relaxation zone structures of a nonreactive, particle-laden, shocked gas wherein the particles are thermally radiative. To quantify the influence of thermal radiation on the re-equilibration process, however, it is necessary first to characterize the behavior of a shocked, particle-laden gas when radiation is neglected. This is accomplished by setting the divergence of the radiative flux in Eq. (10) to zero, which reduces the two-point boundary value problem to an initial value problem starting at the shock front. For convenience, Table 2 presents a comparison of the equations and initial/boundary conditions for both the radiative and nonradiative models presented in this work.

Table 1 Typical input parameters and results for iteration scheme[a]

ω	$X_{f,0}$, m	Ω	$I^-(0)$, W/m^2 – sr	X_f, m	L_{sh}, m	No. of iterations
0.0	5.0	0.9	146.19	7.697	4.936	17
0.5	12.0	0.5	146.22	10.26	6.424	19
0.95	15.0	0.5	146.71	25.27	13.97	18

[a] $M = 4.0$, $d = 20$ μm, $\eta = 0.01$, $\varepsilon_o = 10^{-5}$ K/m.

Table 2 Comparison of solution procedures for nonradiative and radiative cases

Radiation model	Governing equations	Mathematical form of eqs.	Initial/boundary conditions
Nonradiative	Eqs. (9–15)	Initial value problem	Eqs. (23–25)
Radiative	Eqs. (9–15), (30–31), (34)	Two-point boundary value problem	Eqs. (23–25), (32–33)

Results presented in the following sections show both the nonradiative and radiative cases for a range of conditions. To illustrate the flow and temperature structure of a shocked, particle-laden gas, the conditions in Table 3 are identified as typical test cases. The particles have the thermal characteristics of magnesium oxide. Unless otherwise stated in the following discussions, the conditions presented in Table 3 are used as input.

Without Radiation

The dimensionless temperature relaxation zone structure for the test case described by the conditions in Table 3, with $M = 4.0$, $d = 20$ μm, and $\eta = 0.05$, is displayed in Fig. 2, where $\theta_g = T_g/T_0$ and $\theta_p = T_p/T_0$. At the frozen state $X = 0$, the gas is shocked to a dimensionless temperature of $\theta_{g+} = 3.839$ for an initial temperature of $\theta_{g-} = 1.0$. After the shock front, the gas-component temperature reaches a maximum due to the viscous work interaction with the particle-component. The gas-component temperature then decreases due to convective heat transfer to the particle-component. The particle-component temperature starts at θ_{p+} (= 1.0) and increases monotonically toward the gas-component temperature, both temperatures equilibrate at a dimensionless temperature of 3.840. For the case shown, the temperature relaxation zone length is $L_{Te} = 0.44$ m. Previous studies[16,17] have shown that the relaxation zone length is a function of the particulate material thermodynamic properties, diameter, Mach number of the shock front, and mass-flow ratio, that is, $L_{Te} = f(\rho_p, C_{P_p}, d, M, \eta)$.

Table 3 Test case parameters

Flow conditions:
- $P_0 = 1$ atm
- $T_0 = 300$ K
- $M = 1.2$–5.0
- $\eta = 0.001$–0.1

Gas properties:
- Composition: 79% N_2 and 21% O_2

Particle properties:
- $d = 4.0$–50.0 μm
- $M_w = 40.30$ kg/kmole
- $\rho_p = 1000$ kg/m^3
- $\omega = 0$–1.0

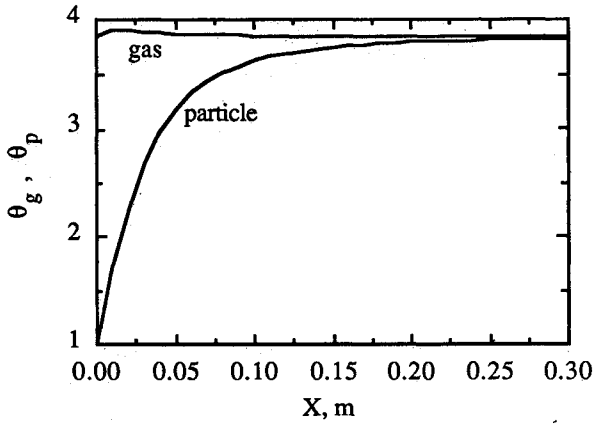

Fig. 2 Temperature relaxation zone structure as a function of the distance relative to the shock front for $M = 4.0$, $d = 20$ μm, and $\eta = 0.05$.

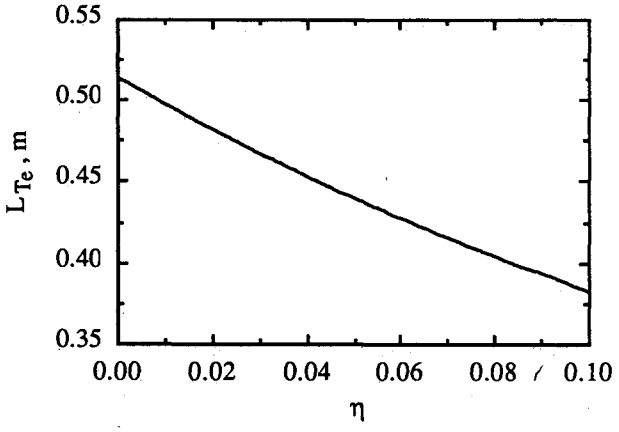

Fig. 3 Variation in the temperature relaxation zone length as a function of the mass-flow ratio for $M = 4.0$ and $d = 20$ μm.

The influence of the mass-flow ratio on the temperature relaxation zone length is shown in Fig. 3. Here, the particle diameter and Mach number are held constant at 20 μm and 4.0, respectively, while the mass-flow ratio is varied from 10^{-6} to 0.10. As the graph shows, L_{Te} reaches a maximum as the mass-flow ratio approaches zero (but not equal to zero where $L_{Te} = 0$). The maximum is a result of the particle-component having negligible influence on the gas-component temperature. That is, with very few particles, the gas-component temperature remains approximately constant throughout the relaxation zone, $0 < X < X_e$. Therefore, a maximum relaxation length is reached as the limit of the number of particles approaches zero. This corresponds to the time for a single particle to increase in temperature to the gas-component temperature. As the mass-flow ratio increases, the particle-component increasingly influences the gas-component temperature. The resulting gas-component temperature peak is greater as the number of particles increases, and the quantity of energy transfer is a direct function of the amount of the particle-component present. As a result, the relaxation zone length decreases as the mass-flow ratio increases.

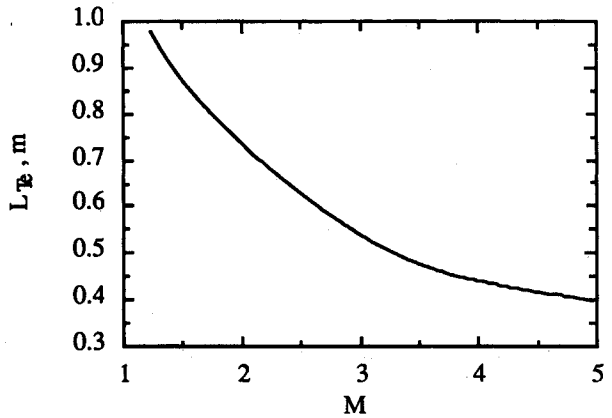

Fig. 4 Temperature relaxation zone length as a function of the Mach number for $d = 20$ μm and $\eta = 0.05$.

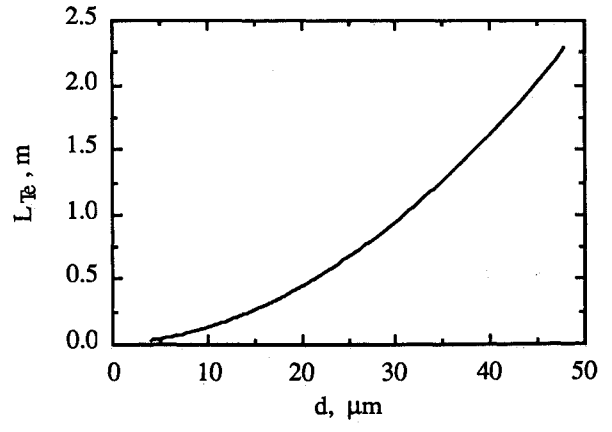

Fig. 5 Temperature relaxation zone length as a function of the particle diameter for $M = 4.0$ and $\eta = 0.05$.

The variation in the temperature relaxation zone length with the Mach number of the shock front is shown in Fig. 4. For this case, the parameters in Table 3 are held constant with $d = 20\ \mu m$, $\eta = 0.05$, and the Mach number varies from $1.2 < M < 5.0$. As shown in the figure, the relaxation zone length decreases as the Mach number increases. This implies that as the Mach number increases, there is an increased driving potential for the mixture to re-equilibrate.

The variation in the temperature relaxation zone with the particle diameter is shown in Fig. 5. Here, the particle diameter was varied from $4 < d\ (\mu m) < 50$, while $M = 4.0$ and $\eta = 0.05$. The relaxation zone length increases approximately proportionally to the particle diameter squared. This is due to the thermal capacity of a particle being proportional to the volume of the particle (or the diameter cubed), whereas the convective heat transfer is a function of the particle surface area (or the diameter squared).

With Radiation

When particle radiation is considered, the length of the preheating zone measured ahead of the shock front L_{sh} is of interest. This length is defined as the distance upstream of the shock front to the point where the particle temperature gradient is equal to 10^{-3} K/m. Preheating zone lengths for $d = 20\ \mu m$, $M = 4.0$, and $\eta = 0.001$ and 0.01 are presented in Fig. 6 as a function of the single scattering albedo. For $\omega = 0$, the results are for absorbing and emitting particles. For $\omega = 1.0$, only particle scattering is considered and the radiation analysis is decoupled from the particle energy equation. Thus, the results for the nonradiating case, where $L_{sh} = 0$, are obtained. The curves exhibit similar characteristics, namely, as the scattering albedo increases, the preheating zone length increases, reaches a maximum, and then decreases (not shown). The increase is particularly rapid as the albedo approaches unity. Maxima of the preheating zone length of 106 and 20.7 m occur near $\omega = 0.99$ for $\eta = 0.001$ and 0.01, respectively. The increase of the preheating length with albedo is due to reduced absorption of the particles, thereby allowing more radiation to be propagated further upstream of the shock.

As the mass-flow ratio increases from 0.001 to 0.01, more particles enter the system and prevent the radiation from propagating upstream with a resultant decrease of the preheating length for a given value of the scattering albedo. When $\omega = 0$, the preheating lengths are 44.7 and 4.9 m for $\eta = 0.001$ and 0.01, respectively. As the mass-flow ratios decreases, the preheating length continues to increase. This is attributed to the mixture becoming optically thin, thereby allowing the radiant energy from the thick porous plug at the equilibrium temperature T_e to pass through the mixture.

To illustrate further the effect of particle radiation, dimensionless gas and particle temperatures immediately in front of the shock $X = X_{f-}$ as a function of the scattering albedo are displayed in Table 4 for $\eta = 0.001$ and 0.01. The Rankine-Hugoniot jump conditions for the gas are applied to the gas temperatures shown in Table 4. For the considered conditions, the effect of particle radiation on the gas temperature is minimal. For the results in the table, the maximum effect on the particle temperature at the shock front is an increase of 14.9 K found at $\omega = 0$ and $\eta = 0.001$.

The influence of the scattering albedo on the temperature relaxation zone length is shown in Fig. 7 for $\eta = 0.001$ and 0.01, for $M = 4.0$, and $d = 20\ \mu m$, where L_{Tea} designates the temperature relaxation zone length in the absence of radiation (Fig. 2). For $\eta = 0.001$ and 0.01, relaxation lengths without radiation are 0.52 and 0.5 m, respectively. For $\eta = 0.001$, the relaxation length for $\omega = 0.0$ is more than four times longer than that without radiation. The relaxation length for radiating particles decreases as the scattering albedo increases and equals that for nonradiating particles when the particles are purely scattering. Increased particle loading indicated by higher values of the mass-flow ratio yield shorter relaxation lengths.

The effect of particle diameter on the temperature relaxation zone length is illustrated in Fig. 8 for scattering albedo from 0.0 to 1.0 for $M = 4.0$ and $\eta = 0.001$. Results for $\omega = 1.0$ display similar characteristics as those for the nonradiating particles in Fig. 5. The relaxation length increases as the particle diameter increases. As the albedo increases from 0 to 1.0, the relaxation lengths monotonically approach those for the nonradiating particles. The major effect of the albedo appears for albedos between 0.5 and 0.9. For $\omega = 0.9$ and 1.0, relaxation lengths are nearly identical.

Table 4 Dimensionless gas and particle temperatures at X_{f-} for $M = 4.0$ and $d = 20\ \mu m$

a) $\eta = 0.001$

ω	θ_{g-}	θ_{p-}
0.0	1.0002	1.0496
0.2	1.0002	1.0411
0.4	1.0002	1.0324
0.6	1.0002	1.0240
0.8	1.0001	1.0150
1.0	1.0000	1.0000

b) $\eta = 0.05$

ω	θ_{g-}	θ_{p-}
0.0	1.0000	1.0114
0.2	1.0000	1.0102
0.4	1.0000	1.0088
0.6	1.0000	1.0071
0.8	1.0000	1.0048
1.0	1.0000	1.0000

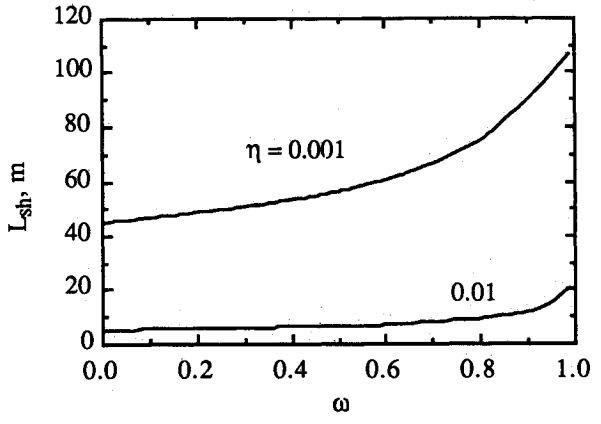

Fig. 6 Effect of scattering albedo on preheating zone length for $M = 4.0$ and $d = 20\ \mu m$.

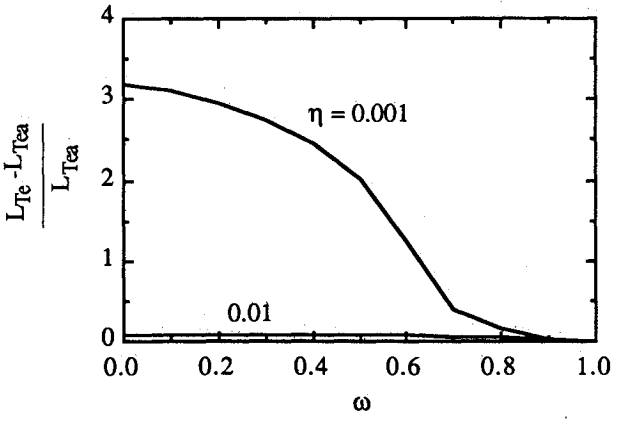

Fig. 7 Effect of scattering albedo on temperature relaxation zone length for $M = 4.0$ and $d = 20\ \mu m$.

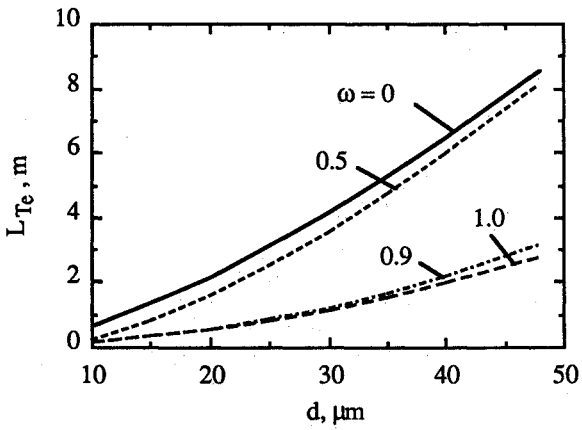

Fig. 8 Effect of particle diameter and scattering albedo on temperature relaxation zone length for nonradiating and radiating cases with $M = 4.0$ and $\eta = 0.001$.

This latter finding differs from that for the preheating lengths displaced in Fig. 6.

The effects of particle radiation on gas and particle temperatures may be more pronounced for reacting systems that produce higher temperatures downstream of the shock.

Conclusions

The primary objective of this research is to investigate the propagation of a shock wave through a particle-laden gas and to determine the preheat and relaxation zone structures for a thermally radiative system. The preheat zone is the region upstream of the shock where the two components (gas and particle) are initially in equilibrium. The relaxation zone is the region following a shock front where the two components exist initially behind the shock at different states (velocity and temperature) and intercomponent transport drives the two components toward equilibrium with each other.

The structure of the preheat and relaxation zones is investigated by applying the conservation principles to a control volume. This approach yields the differential form of the governing equations. The radiative transport within the particle cloud is developed using the two-flux model. The resulting equations form a set of nonlinear, ordinary differential equations that describe the velocity and temperature variation of both the gas and particle components as well as the density and pressure variation in the gas component and the concentration changes for the particle component. To close this system of equations, initial conditions are stated far upstream of the shock, the conditions across the shock front are described by the Rankine-Hugoniot shock relations for the gas component, and the final conditions for the radiant intensity are stated far downstream of the shock.

For several test cases, the governing equations are integrated from the initial state to final state where the differences in the velocities and temperatures are relaxed, implying that the mixture exists in complete equilibrium. The form of the intercomponent transport terms for momentum and energy transfer does not influence the equilibrium state that is reached, but it does influence the structure of the preheating and relaxation zones.

Results reported for nonradiating particles serve as a basis of comparison for radiating particles. For radiating particles, the preheating zone length increases, reaches a maximum, and returns to the nonradiating particle result as the scattering albedo increases. Except for the purely scattering particles, radiating particles increase the relaxation zone length. The extension of the relaxation length is important when considering the minimum (or critical) cell size required to propagate a steady-state Chapman-Jouguet detonation in a fuel-air cloud.

The model developed for particle-laden, shocked gas systems provides useful information about the trends in the preheating and relaxation zone of multicomponent inert systems. In future work, the model should be extended to include a temperature distribution in the particles that exists when the Biot number of the particles is large. It is also recognized that a bow shock may form in front of the particles shortly after the shock. The formation of the bow shock can influence the particle temperature and velocity, thus affecting the form of the intercomponent transport terms. Extension of the radiation model to include effects of polydispersions, anisotropic scattering, gas radiation, and nongray radiation should be considered in future studies. Reacting systems with the potential to produce high temperatures downstream of the shock need to be examined. To this end, ignition and combustion models as well as radiative property models for multiphase and multicomponent particles need to be developed. Finally, experimental verification of the findings of these studies needs to be performed.

Acknowledgments

This work was supported by the Naval Weapons Center, China Lake, California, Contract N60530-89-C-0383.

References

[1]Carrier, G. F., "Shock Wave in a Dusty Gas," *Journal of Fluid Mechanics*, Vol. 4, Pt. 4, 1958, pp. 376–382.

[2]Zink, W., "Attenuation of Sound by Solid Particles Suspended in a Gas," CR 51-0796, Physics Dept., UCLA, 1957.

[3]Campbell, I. J., and Pitcher, A. S., "Shock Waves in a Liquid Containing Gas Bubbles," *Proceeding of the Royal Society of London, Series A: Mathematical and Physical Sciences*, Vol. 243, No. 1, 1958, pp. 145–171.

[4]Morgenthaler, J. H., "Analysis of Two-Phase Flow in Supersonic Exhausts," *Detonation in Two-Phase Flow*, Progress in Astronautics and Rocketry Series, Vol. 6, Academic Press, New York, 1962.

[5]Kriebel, A. R., "Analysis of Normal Shock Waves in a Particle-Laden Gas," *Journal of Basic Engineering*, Vol. 86, No. 4, 1964, pp. 655–665.

[6]Rudinger, G., "Some Properties of Shock Relaxation in Gas Flows Carrying Small Particles," *Physics of Fluids*, Vol. 7, No. 5, 1964, pp. 658–663.

[7]Rudinger, G., *Fundamentals of Gas-Particle Flow*, Elsevier, New York/Amsterdam, 1980.

[8]Rudinger, G., "Some Effects of Finite Particle Volume on the Dynamics of Gas-Particle Mixture," *AIAA Journal*, Vol. 3, No. 7, 1965, pp. 1217–1222.

[9]Rudinger, G., "Relaxation in Gas-Particle Flow," *Non-Equilibrium Flows*, edited by P. P. Wegener, Vol. 1, Pt. 1, Marcel Dekker, New York, 1969, pp. 119–161.

[10]Varma, T. D., and Chopra, N. K., "Analysis of Normal Shock Waves in a Gas-Particle Mixture," *Zeitschrift fuer Angewandte Mathematik und Physik*, Vol. 18, No. 4, 1967, pp. 650–660.

[11]Krier, H., and Mozaffarian, A., "Two-Phase Reactive Particle Flow Through Normal Shock Waves," *International Journal of Multiphase Flow*, Vol. 4, No. 1, 1977, pp. 65–79.

[12]Elperin, I., Igra, O., and Ben-Dor, G., "Analysis of Normal Shock Waves in a Carbon Particle-Laden Oxygen Gas," *Journal of Fluids and Engineering*, Vol. 108, No. 3, 1986, pp. 354–359.

[13]Ben-Dor, G., and Igra, O., "The Relaxation Zone Behind Normal Shock Waves in a Reacting Dusty Gas. Part 1: Monatomic Gases," *Journal of Plasma Physics*, Vol. 27, No. 3, 1982, pp. 377–395.

[14]Igra, O., and Ben-Dor, G., "The Relaxation Zone Behind Normal Shock Waves in a Reactive Dusty Gas. Part 2: Diatomic Gases," *Journal of Plasma Physics*, Vol. 31, No. 1, 1984, pp. 115–140.

[15]Rakib, Z., Igra, O., and Ben-Dor, G., "The Effect of Water Droplets on the Relaxation Zone Developed Behind Strong Normal Shock Waves," *Journal of Fluids and Engineering*, Vol. 106, No. 2, 1984, pp. 154–159.

[16]Yao, J. Z., "Analysis of Particle-Laden Gaseous Shock Waves," Ph.D. Thesis, The Univ. of Iowa, Iowa City, IA, 1989.

[17]Butler, P. B., and Schmitt, R. G., "Shock Propagation Through a Perfect Gas Entrained with a Normal Distribution of Fine Particles," *Power Technology*, Vol. 63, No. 3, 1991, pp. 224–240.

[18]Baek, S. W., and Seung, S., "On the Postshock Flow Field of Carbon Particle Laden Gases," *Combustion and Flame*, Vol. 75, No. 3, 1989, pp. 255–263.

[19]Baek, S. W., and Seung, S., "Parametric Analysis On the PostShock

Wave Relaxation of Carbon Particle Laden Gases," *Combustion and Flame*, Vol. 80, No. 2, 1990, pp. 126–134.

[20]Chase, M. W., Davies, C. A., Downey, J. R., Frurip, D. J., McDonald, R. A., and Syverud, A. N., *JANNAF Thermochemical Tables*, 3rd ed., American Chemical Society, New York, 1985.

[21]Incropera, F. P., and DeWitt, D. P., *Fundamentals of Heat and Mass Transfer*, Wiley, New York, 1985.

[22]Siegel, R., and Howell, J. R., *Thermal Radiation Heat Transfer*, 2nd ed., Hemisphere, New York, 1981.

[23]Özisik, M. N., *Radiative Transer*, Wiley, New York, 1973.

[24]Brewster, M. Q., and Tien, C. L., "Examination of the Two-Flux Model for Radiative Transfer in Particulate Systems," *International Journal of Heat and Mass Transfer*, Vol. 25, No. 12, 1982, pp. 1905–1907.

[25]Bohren, C. F., and Huffman, D. R., *Absorption and Scattering of Light by Small Particles*, Wiley, New York, 1983.

[26]Kamiuto, K., "The Diffraction-Scattering Subtraction Method for Highly Anisotropic Scattering Problems," *Journal of Quantitative Spectroscopy & Radiative Transfer*, Vol. 40, No. 1, 1988, pp. 21–28.

[27]Hindmarsh, A. C., *LSODE (integration package)*, Mathematics and Statistics Section, L-300, Lawrence Livermore Lab., Livermore, CA, 1980.

[28]Conte, S., and de Boor, C., *Elementary Numerical Analysis*, McGraw-Hill, New York, 1980.